PREDICTION OF FREE SURFACE FLOW ON CONTAINMENT FLOOR USING A SHALLOW WATER EQUATION SOLVER

YOUNG SEOK BANG*, GIL SOO LEE, BYUNG-GIL HUH, DEOG-YEON OH and SWENG-WOONG WOO
Korea Institute of Nuclear Safety
P.O. Box 114, Yuseong, Daejeon, 305-335, Korea
*Corresponding author. E-mail : k164bys@kins.re.kr

Received January 19, 2009
Accepted for Publication June 10, 2009

A calculation model is developed to predict the transient free surface flow on the containment floor following a loss-of-coolant accident (LOCA) of pressurized water reactors (PWR) for the use of debris transport evaluation. The model solves the two-dimensional Shallow Water Equation (SWE) using a finite volume method (FVM) with unstructured triangular meshes. The numerical scheme is based on a fully explicit predictor-corrector method to achieve a fast-running capability and numerical accuracy. The Harten-Lax-van Leer (HLL) scheme is used to reserve a shock-capturing capability in determining the convective flux term at the cell interface where the dry-to-wet changing proceeds. An experiment simulating a sudden break of a water reservoir with L-shape open channel is calculated for validation of the present model. It is shown that the present model agrees well with the experiment data, thus it can be justified for the free surface flow with accuracy. From the calculation of flow field over the simplified containment floor of APR1400, the important phenomena of free surface flow including propagations and interactions of waves generated by local water level distribution and reflection with a solid wall are found and the transient flow rates entering the Holdup Volume Tank (HVT) are obtained within a practical computational resource.

KEYWORDS : Free Surface Flow, Containment Floor, Shallow Water Equation, Finite Volume Method

1. INTRODUCTION

Following a loss-of-coolant accident (LOCA) in a pressurized water reactor (PWR), the water discharged from the break spreads over the containment floor in a transient manner. The high velocity of water flow just after the break is significantly reduced by impingement on the structural wall and by friction with the dry floor and the flow direction may be changed by the reflective waves from the various structural walls of the containment. Those phenomena in a free surface flow with complex geometry may have an impact on the prediction of the transport of debris generated by LOCA [1].

The recent calculations of the flow field on a containment floor for the use of debris transport were mostly in a steady state [2-4], while transient free surface flow has been attempted in a limited scope in debris transport studies [5]. This may be because the important information on debris transport can be obtained by the steady state flow calculation instead of a complicated transient calculation since most PWR have a switchover process from injection mode to recirculation mode of its emergency core cooling system (ECCS). However, for some of the advanced PWR designs that do not have a change in the ECCS water source [6], debris transport is no longer in a steady state and a transient calculation should be considered at least for the duration from the break initiation until the time that flow driven by the break flow is balanced by the ECCS pump suction flow.

Commercial computational fluid dynamics (CFD) codes can be used for the calculation of transient free surface flow. As a typical case, the FLUENT code [7] has been used for prediction of the transient flow field in a simplified containment domain [8]. It provided detailed information of the flow field but it usually took a significant effort for mesh generation and a huge amount of computational time (more than one month) even for short-term calculation in a super computer. It implied that the current computational environment using CFD technology to calculate transient free surface flow in complex geometry still has to be improved to be practical, especially for the use of safety evaluation on debris transport, although the computational speed is being increased.

Recently, two-dimensional shallow water equations (SWE) [9] instead of full three-dimensional Navier-Stokes equations have been used to calculate the free surface flow in environmental engineering [10,11]. The advantage of

this approach is a capability to cover a relatively large-scale domain such as a river and to use a simple computational algorithm of a hyperbolic conservation equation. Such an approach may be applied to the problem of containment, based on the similarity between flooding of a floodplain and a break flow in a dry containment floor.

In the present study, a calculation model based on the SWE and an explicit finite volume method (FVM) was developed to predict the transient flow field in sufficient reliability and accuracy within a reasonable computational resource. Unstructured triangular mesh was used to represent the complex geometry in the PWR containment floor [12]. In this kind of calculation, a special shock-capturing numerical scheme is needed to simulate hydraulic jump and steep wave propagation, especially near the break region and wet-dry interface. For this aspect, the Harten-Lax-van Leer (HLL) scheme was used as an approximate Riemann solver [13]. The fully explicit predictor-corrector scheme [14] was also adopted to reserve the numerical accuracy in time. The present paper describes the model, validates the model with applicable experimental data, and discusses its application to the calculation of flow field over a simplified PWR containment floor of the Advanced Power Reactor 1400 (APR1400) [6].

2. CALCULATION MODEL

2.1 Governing Equation

From the Navier-Stokes equation, two-dimensional shallow water equation (SWE) can be obtained by assuming vertical velocity and related shear stresses being neglected and by integrating the continuity equation and x and y momentum equations in the z direction over depth h from bed to free surface [9]. The resulting SWE is as follows:

$$\frac{\partial \boldsymbol{U}}{\partial t}+\frac{\partial \boldsymbol{F}}{\partial x}+\frac{\partial \boldsymbol{G}}{\partial y}=\frac{\partial \boldsymbol{R}_x}{\partial x}+\frac{\partial \boldsymbol{R}_y}{\partial y}+\boldsymbol{S} \tag{1}$$

$$\boldsymbol{U}=\begin{bmatrix} h \\ hu \\ hv \end{bmatrix},\ \boldsymbol{F}=\begin{bmatrix} hu \\ hu^2+1/2gh^2 \\ huv \end{bmatrix},\ \boldsymbol{G}=\begin{bmatrix} hv \\ huv \\ hv^2+1/2gh^2 \end{bmatrix} \tag{2a}$$

$$\boldsymbol{R}_x=\begin{bmatrix} 0 \\ \nu_e(\partial hu/\partial x) \\ \nu_e(\partial hv/\partial x) \end{bmatrix},\ \boldsymbol{R}_y=\begin{bmatrix} 0 \\ \nu_e(\partial hu/\partial y) \\ \nu_e(\partial hv/\partial y) \end{bmatrix},\ \boldsymbol{S}=\begin{bmatrix} B(t) \\ gh(S_{ox}-S_{fx}) \\ gh(S_{oy}-S_{fy}) \end{bmatrix} \tag{2b}$$

$$S_{ox}=-\frac{\partial z_b}{\partial x},\ S_{oy}=-\frac{\partial z_b}{\partial y} \tag{2c}$$

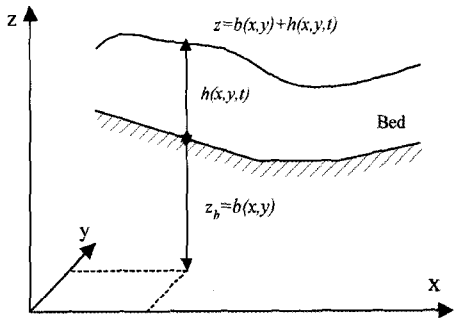

Fig. 1. Definition of Shallow Water Equation

$$S_{fx}=\frac{un_m^{\,2}\sqrt{u^2+v^2}}{h^{4/3}},\ S_{fy}=\frac{vn_m^{\,2}\sqrt{u^2+v^2}}{h^{4/3}} \tag{2d}$$

where h, u, v, and z_b denote water level from the bed, velocity components in x and y directions, and bed elevation, respectively. And n_m, $B(t)$, and ν_e are the Manning bed friction coefficient ($m^{-1/3}s$), water source term into flow field, and depth-averaged effective viscosity, respectively. The source terms in the right-hand side of Eq. (1) are due to the mass added by $B(t)$, the momentum induced by the bed slope (S_o), and the momentum lost by friction with the bed (S_f) of water, respectively. Eq. (1) is a hyperbolic equation in which the initial condition is propagated by time and space and the discontinuous solution such as shock can be involved. Generally, a numerical solution is attempted for Eq. (1) due to the discontinuity and the complex geometry to be solved.

2.2 Numerical Model

The integral form of Eq. (1) over the area A surrounded by a closed path C can be expressed as follows:

$$\int_A \frac{\partial \boldsymbol{U}}{\partial t}dA+\int_C(\boldsymbol{F}n_x+\boldsymbol{G}n_y)dC=\int_C(\boldsymbol{R}_x n_x+\boldsymbol{R}_y n_y)dC+\int_A \boldsymbol{S}dA \tag{3}$$

where n_x and n_y mean the x- and y-component of the outward unit normal vector on C, respectively. Assuming $\boldsymbol{U}$ is a constant within an area A_k having a triangular shape (Fig. 2), the finite volume discretized form of Eq. (3) can be obtained.

$$A_k\frac{d\boldsymbol{U}_k}{dt}+\sum_{j=1}^{3}\left[\boldsymbol{F}_{kj}n_{xj}+\boldsymbol{G}_{kj}n_{yj}\right]L_j=\sum_{j=1}^{3}\left[\boldsymbol{R}_{xkj}n_{xj}+\boldsymbol{R}_{ykj}n_{xj}\right]L_j+A_k\boldsymbol{S}_k \tag{4}$$

where j, L_j, n_{xj}, and n_{yj} denote side numbers of a triangular cell, length of side j, component of unit normal vector in x and one in y direction, respectively.

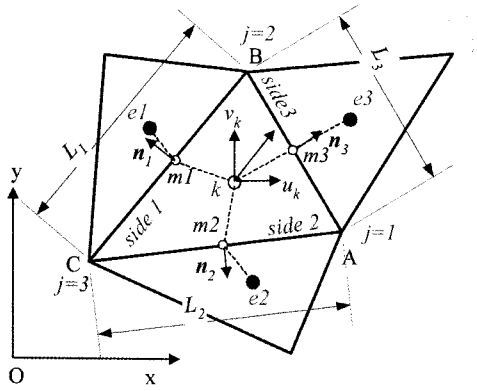

Fig. 2. Notations of Cells, Nodes, and Sides

The time derivative term of Eq. (4) can be expressed by explicit form to get a solution at a new time level using the old time values as follows:

$$\boldsymbol{U}_k^{n+1} = \boldsymbol{U}_k^n - \frac{\Delta t}{A_k}\sum_{j=1}^{3}\left[(\boldsymbol{F}_{kj}^n n_{xj} + \boldsymbol{G}_{kj}^n n_{yj}) - (\boldsymbol{R}_{xkj}^n n_{xj} + \boldsymbol{R}_{ykj}^n n_{yj})\right]L_j + \boldsymbol{S}_k^n \Delta t \quad (5)$$

The superscript n and $n+1$ denote old time and new time and the variable vector, $\boldsymbol{U}$, is calculated at the cell center. In Eq. (5), the convective flux terms ($\boldsymbol{F}_{kj}$, $\boldsymbol{G}_{kj}$) and diffusive flux terms ($\boldsymbol{R}_{x\,kj}$, $\boldsymbol{R}_{y,kj}$) should be defined at each side. They can be approximated by a central difference scheme based on the cell-centered value. However, such an approach may lead to an unphysical oscillation and instability of the solution, especially at the wet-dry interface. To resolve the problem, an approximate Riemann solver, Harten-Lax-van Leer (HLL) scheme [13] was introduced. According to the HLL scheme, the convective flux terms can be described as follows [15]:

$$\boldsymbol{F}^{HLL} = \begin{cases} \boldsymbol{F}(\boldsymbol{U}_L) & if \quad s_L > 0 \\ \boldsymbol{F}^*(\boldsymbol{U}_L, \boldsymbol{U}_R) & if \quad s_L \le 0 \le s_R \\ \boldsymbol{F}(\boldsymbol{U}_R) & if \quad s_R > 0 \end{cases} \quad (6)$$

$$\boldsymbol{F}^*(\boldsymbol{U}_L, \boldsymbol{U}_R) = \frac{1}{s_R - s_L}\left[(s_R \boldsymbol{F}(\boldsymbol{U}_L) - s_L \boldsymbol{F}(\boldsymbol{U}_R))\cdot \boldsymbol{n} + s_L s_R (\boldsymbol{U}_R - \boldsymbol{U}_L)\right] \quad (7)$$

where, subscripts L and R represent the values at the cell left to the interface and at the cell right, respectively. s_R and s_L are the wave speeds at those cells defined by the following equation.

$$s_L = \min(\boldsymbol{V}_L \cdot \boldsymbol{n} - \sqrt{gh_L},\ \boldsymbol{V}^* \cdot \boldsymbol{n} - c^*) \quad (8a)$$

$$s_R = \max(\boldsymbol{V}_R \cdot \boldsymbol{n} - \sqrt{gh_R},\ \boldsymbol{V}^* \cdot \boldsymbol{n} + c^*) \quad (8b)$$

where, velocity vector is $\boldsymbol{V}=u\boldsymbol{i}+v\boldsymbol{j}$. The asterisked variables, $\boldsymbol{V}^*$ and c^*, are defined as follows:

$$\boldsymbol{V}^* \cdot \boldsymbol{n} = \frac{1}{2}(\boldsymbol{V}_L + \boldsymbol{V}_R)\cdot \boldsymbol{n} + \sqrt{gh_L} - \sqrt{gh_R} \quad (9)$$

$$c^* = \frac{1}{2}(\sqrt{gh_L} + \sqrt{gh_R}) + \frac{1}{4}(\boldsymbol{V}_L - \boldsymbol{V}_R))\cdot \boldsymbol{n} \quad (10)$$

In order to reserve the second order numerical accuracy in time, the predictor-corrector method is applied. In the predictor step, the variables at the $n+1/2$ time level are calculated as follows:

$$\boldsymbol{U}_k^{n+\frac{1}{2}} = \boldsymbol{U}_k^n - \frac{\Delta t}{2A_k}\sum_{j=1}^{3}\left[(\boldsymbol{F}_{kj}^n n_{xj} + \boldsymbol{G}_{kj}^n n_{yj}) - (\boldsymbol{R}_{xkj}^n n_{xj} + \boldsymbol{R}_{ykj}^n n_{yj})\right]L_j + \boldsymbol{S}_k^n \frac{\Delta t}{2} \quad (11)$$

where, the convective flux terms are calculated using the central difference scheme (Fig. 2).

$$\boldsymbol{F}_{kj}^n = \frac{d_{kmj}}{d_{kej}}\boldsymbol{F}_k^n + (1 - \frac{d_{kmj}}{d_{kej}})\boldsymbol{F}_{ej}^n \quad (12)$$

where d_{kej}, d_{kmj} mean distance from point k to point ej and one to point mj (Fig. 2), respectively. The corrector step calculates the variables at the $n+1$ time level, using the $\boldsymbol{U}$ calculated by predictor step and the flux terms determined by HLL scheme using Eqs. (6)~(10).

$$\boldsymbol{U}_k^{n+1} = \boldsymbol{U}_k^{n+\frac{1}{2}} - \frac{\Delta t}{2A_k}\sum_{j=1}^{3}\{(\boldsymbol{F}^{HLL^{n+\frac{1}{2}}}_{kj} n_{xj} + \boldsymbol{G}^{HLL^{n+\frac{1}{2}}}_{kj} n_{yj}) - (\boldsymbol{R}_{xkj}^{n+\frac{1}{2}} n_{xj} + \boldsymbol{R}_{ykj}^{n+\frac{1}{2}} n_{yj})\}L_j + \boldsymbol{S}_k^{n+\frac{1}{2}}\frac{\Delta t}{2} \quad (13)$$

For the diffusive flux term, simple distance-weighted differencing scheme is applied as follows (Fig. 2):

$$\boldsymbol{R}_x|_{Side-j} = \nu_e \left.\frac{\partial \boldsymbol{U}}{\partial x}\right|_j = \nu_e\left\{\left.\frac{\partial \boldsymbol{U}}{\partial x}\right|_k^{mj}\frac{\Delta x_{ej-mj}}{\Delta x_{k-ej}} + \left.\frac{\partial \boldsymbol{U}}{\partial x}\right|_{mj}^{e_j}\frac{\Delta x_{mj-k}}{\Delta x_{k-ej}}\right\} = \nu_e\left\{\frac{\boldsymbol{U}_{mj} - \boldsymbol{U}_k}{x_{mj} - x_k}\frac{x_{ej} - x_{mj}}{x_k - x_{ej}} + \frac{\boldsymbol{U}_{ej} - \boldsymbol{U}_{mj}}{x_{ej} - x_{mj}}\frac{x_{mj} - x_k}{x_k - x_{ej}}\right\} \quad (14)$$

where, $\Delta x_{k\text{-}ej}$ and x_{ej} mean the distance in x direction between

point k and point ej and the x coordinate of the point ej (j=1,2,3). The same differencing scheme is applied to $\boldsymbol{R}_{yj}$. The depth-averaged effective viscosity, v_e, includes kinematic viscosity and turbulent eddy viscosity. Turbulent eddy viscosity was not specifically modeled for simplicity. The source term, mainly related to the water addition to the calculation system such as break flow, can also be easily approximated.

The time step size in Eqs. (11) and (13) should be limited to prevent a negative water level [14]:

$$\Delta t \le K_{CFL} Min_k \left(\frac{A_k}{Max_j \left| \boldsymbol{V} \cdot \boldsymbol{n} \pm \sqrt{gh} \right|_{kj} L_j} \right) \tag{15}$$

where K_{CFL} is the Courant-Fredrich-Lewy (CFL) number and is set to 0.7 in this study.

2.3 Boundary Conditions

Four types of boundary conditions were considered in the present model: (1) no-slip wall, (2) slip wall, (3) open boundary, and (4) flow rate-imposed boundary. For all the cases, the water level (h) at the side is set to the same as one of the associated cell centers (h_j=h_k). For the no-slip wall, zero velocity is imposed at the side representing the wall (u_j= v_j=0). For the slip wall, only the component tangential to the wall from velocity at the associated cell center is imposed to the side. For the open boundary, velocity at the side is set to the same as one of the associated cells (Fig. 3).

The flow rate-imposed boundary, case (4), considers the actual situation of the containment sump pit having a discontinuous bed elevation from the nearby cells. It was assumed that the flow rate at the boundary can be specified by the function of the water level. The following formula for the broad crested weir case [16] is used.

$$u = \frac{Q_{BCW}}{hL_x}, v = \frac{Q_{BCW}}{hL_y}, \quad Q_{BCW} = \left(\frac{2}{3}\right)^{3/2} g^{1/2} h^{3/2} \tag{16}$$

where L_x, and L_y represent the length of the boundary side in x and one in y direction, Q_{BCW} is the flow rate at the broad crested weir, and h is taken from the center of the adjacent cell upstream.

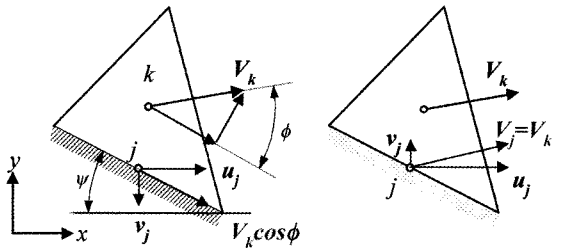

a) slip boundary b) open boundary

Fig. 3. Treatment of Boundary Condition

3. RESULT AND DISCUSSION

3.1 Model Validation

To confirm the applicability and validity of the present model, the experiment described in the reference [9] was calculated. Fig. 4 shows the experiment setup. The reservoir was a 2.4 ×2.4m rectangular shape and was initially filled with 0.2 m of water. An L-shaped open channel was connected to the reservoir and was in a dry state. A gate in front of the pool was instantaneously ruptured and water was driven into the dry channel. The water level was measured at several locations as in Fig. 4. Computational meshes were generated using the EASYMESH [17] as shown in Fig. 4.

The total number of cells, nodes, and sides were 1238, 2231, and 3468, respectively. Cell size was almost 0.1 m.

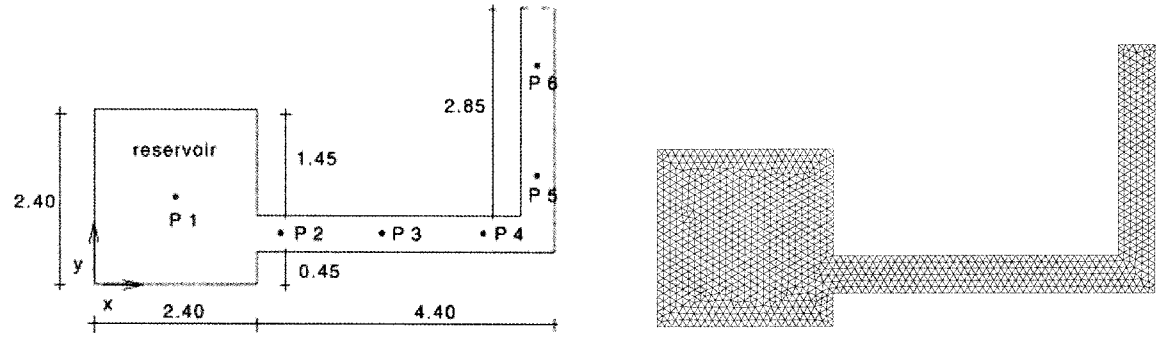

Fig. 4. Experiment Setup and Computational Mesh

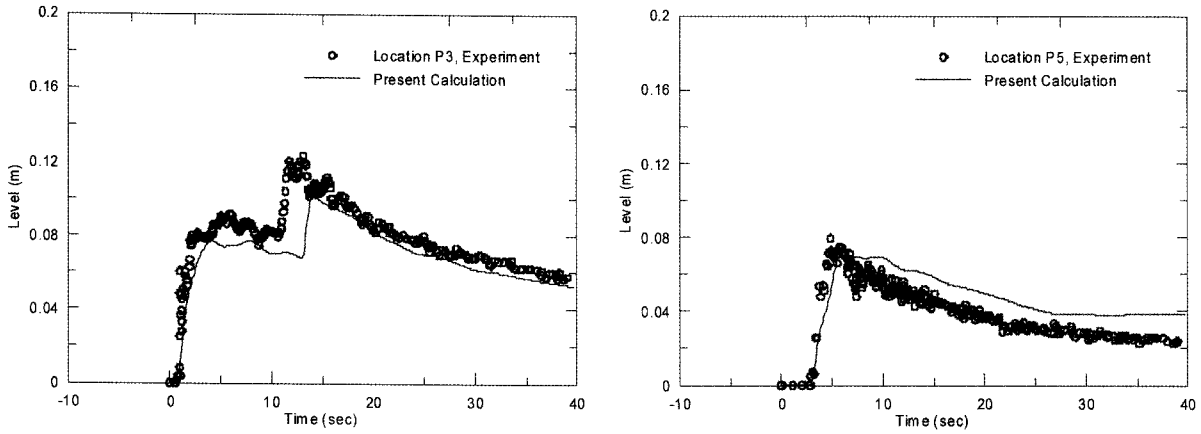

Fig. 5. Comparison of Water Level at Points P3 and P5

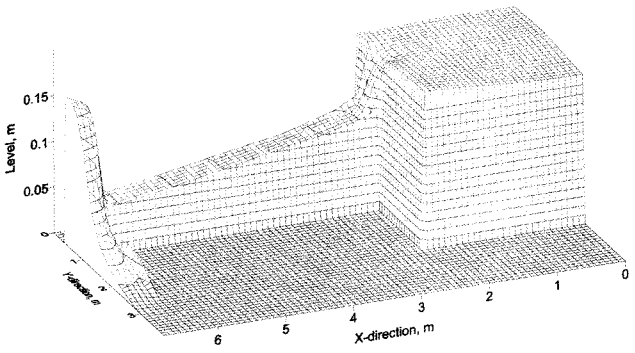

Fig. 6. Configuration of Local Water Level at 3.7 sec

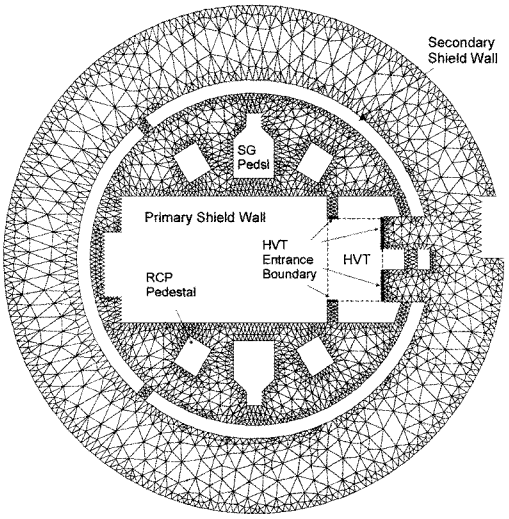

Fig. 7. Mesh System of the APR-1400 Containment Floor

At the exit of the L-shaped channel and at the all wall boundaries, the open boundary condition and no-slip condition were imposed, respectively.

Fig. 5 shows the calculated water level at points P3 (4.25, 0.70 m) and P5 (6.55, 1.50 m). The calculated behavior of the water level was close to the measured data. Especially the time of change from dry to wet at each point was well predicted. The deviation from the measured data was a time delay, which was due to the difference in location between the calculated and the measured point. Fig. 6 shows a configuration of level distribution in the domain at 3.7 seconds, which indicated the start of the propagation of the reflected wave at the corner of the L-shaped channel and dry-wet interface near the exit of the domain. Those results implied the current model has sufficient validity and accuracy in calculating the free surface flow.

3.2 Calculation of Flow Field over Containment Floor

The transient flow field over a simplified containment floor of the APR1400 was calculated. Fig. 7 shows a computational mesh of the floor, which included several concrete structures and HVT. Concrete structures included the containment inner wall (CIW), the primary and secondary shield walls (PSW and SSW), the steam generator (SG) pedestals, the reactor coolant pump (RCP) pedestals, and the HVT shield wall (HSW). The compartment for the letdown heat exchanger and one for the reactor drain tank were not modeled for simplicity. The computational mesh was composed of 4792 cells, 2996 nodes, and 7798 sides. Due to the geometrical complexity, it was difficult to generate the mesh in a uniform size over the domain. As a result, the mesh size ranged from 0.1 to 1 m. In order to represent the structural wall accurately, finer mesh was used near the solid wall. The HVT entrance boundary was

also simulated by meshes with a small size. Since the size and the uniformity of the mesh may have an effect on the calculations, further study is needed for the confidence of the calculations.

The break flow and the containment spray flow into the containment floor were simulated as a function of time according to the data described in the Safety Analysis Report of the APR1400 [6] as shown in Fig. 8. The containment spray flow was also included to the water source function, $B(t)$. The cells to which the break flow is introduced were designated by a circle. The center of the circle was assumed at the midpoint between the SG-1 pedestal boundary and the PSW boundary and the radius was 1 m. From the break flow data shown in Fig. 8, the water source for each cell was calculated per each time step based on the ratio of the cell area to the circle area. The Manning friction coefficient was set to 0.0095 based on the reference [9]. Calculation was carried out to 100 seconds.

Fig. 9 shows the calculated water level and velocity vectors over the containment floor at times of 3, 8, 16, and 33.5 seconds into transient. After the break was initiated, water poured down the floor and struck the SSW. Dry cells

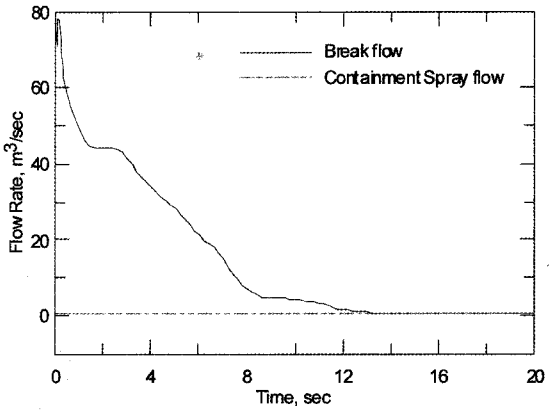

Fig. 8. Break Flow of the APR-1400

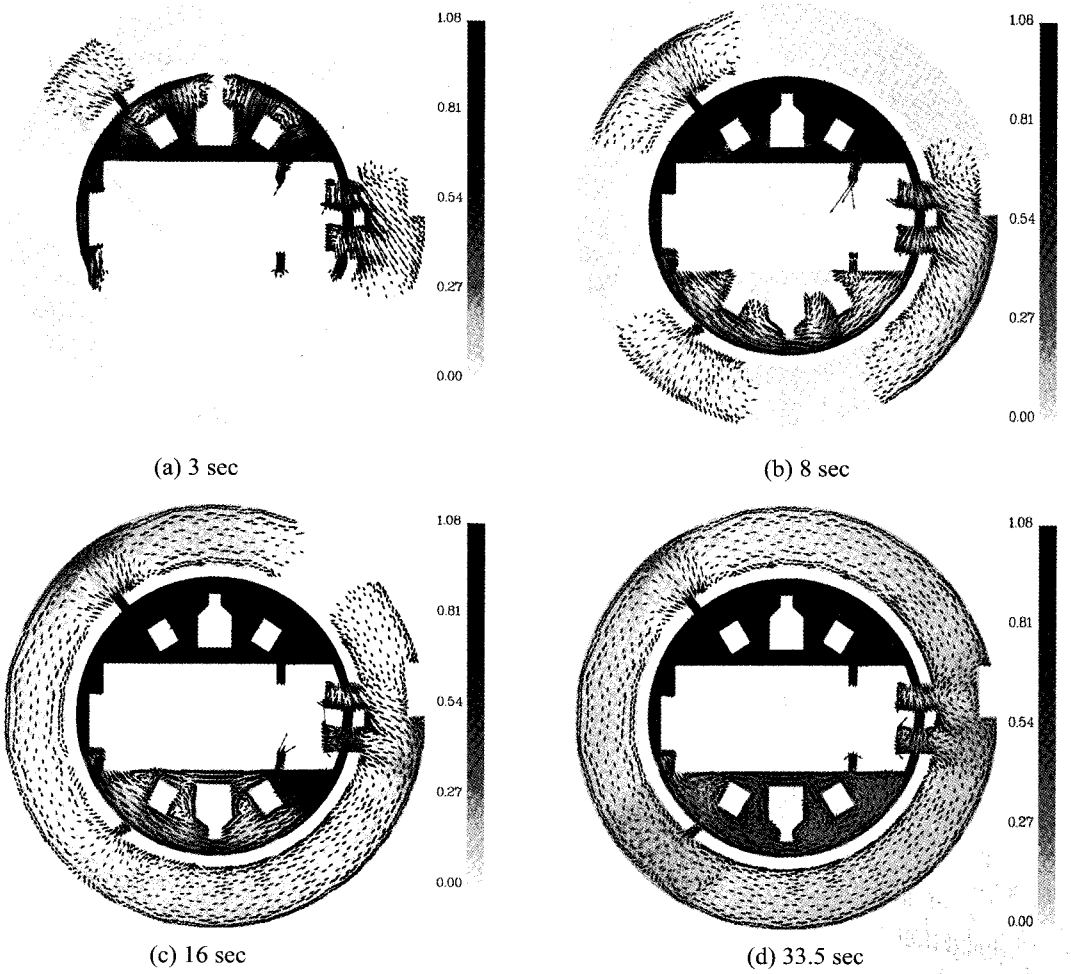

(a) 3 sec (b) 8 sec

(c) 16 sec (d) 33.5 sec

Fig. 9. Calculated Water Level and Velocity Vectors

within the SSW changed to a wet state. The water level inside the SSW increased and the surface wave was reflected to the upstream, as shown in Fig. 9(a). By this mechanism, quadrants 1 and 2 inside the SSW were flooded in 3.2 seconds. Water at quadrant 1 and 2 flowed into the annulus area through the doorway in quadrant 2 and the passage between the HSW and the SSW (Fig.9(b)). At 16 sec, quadrants 3 and 4 were flooded with the water that had escaped from the narrow path between the PSW and the SSW (Fig. 9(c)). As shown in Fig. 9(c), a portion of the water passing through the necking points between the HSW and the SSW was introduced into quadrant 4. This water stream was faced with the stream coming from quadrant 3. The surface wave at the interface propagated counterclockwise, which caused the local circulation of water within the region to become trapped. As the water level of quadrants 3 and 4 inside the SSW increased, the water flow passing through the doorway at quadrant 3 increased and the region at quadrant 3 outside the SSW got much water. It made the local water level increase and the surface wave propagate in clockwise and counterclockwise directions.

Fig. 10 shows the flow rates at the four entrances to the HVT. As expected, the flow rate at entrance 1 was significant. The flow rate at entrance 3 was greater than the one at entrance 2 due to the water level behavior explained above. The water level at entrance 1 of the HVT was initially higher than 1 m and then decreased to 0.25 m in a stabilized manner.

The CPU time required for a 100 second calculation was 4649 seconds (~1.5 hours) in a Pentium IV 3.4 GHz processor. Thus, the present model can be regarded as a significantly practical one when compared to the commercial CFD calculation.

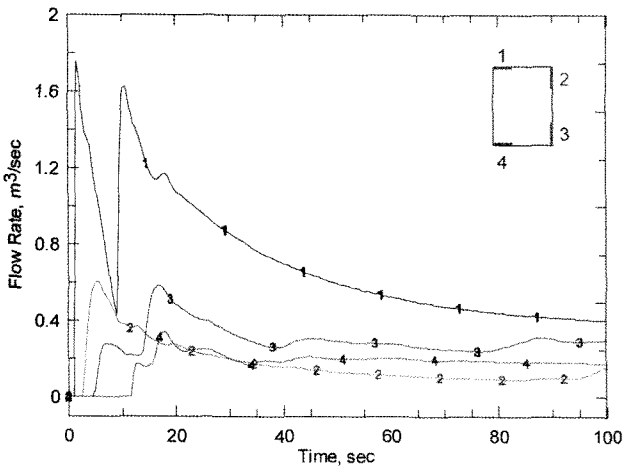

Fig. 10. Calculated Flow Rates to the HVT

4. SUMMARY AND CONCLUSION

A calculation model to predict the transient free surface flow on a PWR containment floor with complex geometry was discussed. The model was based on two-dimensional Shallow Water Equation (SWE) and Finite Volume Method (FVM) with unstructured triangular meshes. The Harten-Lax-van Leer (HLL) scheme was used to predict the dry-to-wet process at the interface and the predictor-corrector scheme was used to reserve the second order accuracy in time. An experiment of a sudden break of a water reservoir with an L-shape open channel was simulated for validation of the present model and the flow field on a simplified containment floor of the APR1400 was calculated. The following conclusions were obtained: 1) From the agreement with the measured water level of the open channel, the applicability and accuracy of the present model was justified for the free surface flow with a dry-to-wet changing process. 2) From the calculated flow field on a containment floor following LOCA, the propagations and interactions of the waves generated by local water level distribution and the reflection with a solid wall were found as important phenomena and the transient flow rates entering the Holdup Volume Tank (HVT) can be calculated within a practical computational resource.

NOMENCLATURE

A	area
$B(t)$	Added water mass in Eq. (1)
C	closed path surrounding A
d_{kej}	distance from point k to point ej
$e1, e2, e3$	three triangular cells surrounding cell k
$\boldsymbol{F}, \boldsymbol{G}$	convective flux vector
g	gravitational acceleration
h	water level
K_{CFL}	coefficient of time step
L_j	length of side j
$m1, m2, m3$	centers of three sides of cell k
n_m	Manning friction coefficient
$\boldsymbol{n}_x, \boldsymbol{n}_y$	components of unit normal vector
Q_{BCW}	flow rate at broad crested weir
$\boldsymbol{R}_x, \boldsymbol{R}_y$	diffusive vector
$\boldsymbol{S}$	source term vector
s	wave speed
t	time
$\boldsymbol{U}$	variable vector
$\boldsymbol{V}$	velocity vector
u, v	x, y component fluid velocity
z_b	bed elevation
Δt	time step size
v_e	depth-averaged effective viscosity

Subscript

BCW	broad crested weir
f	friction
i, j, k	index of node, side, cell

L, R	left and right
o	bed slope
m	Manning
x, y, z	rectangular coordinates

Superscript

HLL	Harten-Lax-van Leer
n	old time
$n+\frac{1}{2}$,	intermediate time
n+1	new time
*	intermediate state for wave speed in HLL scheme

ABBREVIATION

APR	Advance Power Reactor
BCW	Broad Crested Weir
CFD	Computational Fluid Dynamics
CIW	Containment Inner Wall
ECCS	Emergency Core Cooling System
FVM	Finite Volume Method
HLL	Harten-Lax-van Leer
HSW	Holdup Volume Tank Shield Wall
HVT	Holdup Volume Tank
LOCA	Loss-ofi-Coolant Accident
PSW	Primary Shield Wall
PWR	Pressurized Water Reactors
RCP	Reactor Coolant Pump
SG	Steam Generator
SSW	Secondary Shield Wall
SWE	Shallow Water Equations

REFERENCES

[1] Rao D. V., et al., 2003, "Knowledge Base for the Effect of Debris on Pressurized Water Reactor Emergency Core Cooling Sump Performance," NUREG/CR-6808, USNRC, (2003).

[2] Maji A. K., et al., "Experimental Validation of CFD Analyses for Estimating the Transport Fraction of LOCA-Generated Insulation Debris to ECCS sump Screens," *Nuclear Technology*, **146**, 3, (2004).

[3] Kim J., et al., "Three Dimensional CFD Analysis on Containment Pool Recirculation in ECCS Sump Performance Evaluation," *Proc. Korean Nuclear Society*, Cheju, Korea, May 10~11, 2007

[4] Lee S. W., et al., "Preliminary CFD Analysis on Debris Transport to ECCS Sump in Recirculation Mode for Kori Unit 3," *Proc. Korean Nuclear Society*, Pyungchang, Korea, Oct. 30~31, 2008

[5] Kim J., et al., "Assessment on Recirculation Sump Performance for PWR Equipped with IRWST," *Proc. Korean Nuclear Society*, Kyeongju, Korea, May 29~30, 2008

[6] KEPCO, 1997, Standard Safety Analysis Report APR-1400, Seoul, Korea. (1997).

[7] ANSYS, FLUENT6.3 Code Manual, Fluent Inc. (2006).

[8] Lee J. I., et al., "Debris Transport Analysis Related with GSI-191 in Advanced Pressurized Water Reactor Equipped with In-containment Refueling Water Storage Tank", *Proceedings of Experiment and Computational Fluid Dynamics for Nuclear Reactor Safety (XCFD4NRS)*, Grenoble, France, Sep.10~12, 2008.

[9] Gottardi G., et al., "Central Scheme for Two-Dimensional Dam-break Flow Simulation," *Advances in Water Resources*, **27** (2004).

[10] Begnudelli L., et al., "Unstructured Grid Finite-Volume Algorithm for Shallow-Water Flow and Scalar Transport with Wetting and Drying," *ASCE Journal of Hydraulic Engineering*, **132**, 4 (2006).

[11] Valerio C., et al., "Finite Volume Method for Simulating Extreme Flood Events in Natural Channels," *Journal of Hydraulic Research*, **41**, 2, (2003).

[12] Bang Y. S., et al., "Transient Flow Field in Containment Floor Following a LOCA of APR-1400," *Proc. Korean Nuclear Society*, Pyungchang, Korea, Oct. 30~31, 2008

[13] Harten A., Lax P. D., and van Leer B., "On Upstream Differencing and Godunov-type Schemes for Hyperbolic Conservation Laws," *SIAM Review*, 25, 1 (1983).

[14] Rogers B. D., et al., "Godunov-type Adaptive Grid Model of Wave-Current Interaction at Cuspate Beaches," *International Journal for Numerical Methods in Fluids*, **46** (2004).

[15] Zhou J. G., et al., "The Surface Gradient Method for the Treatment of Source Terms in the Shallow-Water Equations," *Journal of Computational Physics*, **168** (2001).

[16] American Nuclear Society, "Design Criteria for Protection against the Effects of Compartment Flooding in Light Water Reactor Plants," ANSI/ANS-56.11, La Grange Park, USA, (1988).

[17] http://www-dinma.univ.trieste.it/nirftc/research/easymesh/easymesh.html.